Published in final edited form as:
IEEE Trans Biomed Eng. 2011 February ; 58(2): 235–242. doi:10.1109/TBME.2010.2053928.

Shearwave Dispersion Ultrasonic Vibrometry (SDUV) for measuring prostate shear stiffness and viscosity – An *in vitro* pilot study

F.G. Mitri[Member, IEEE],
Department of Physiology and Biomedical Engineering, College of Medicine, Mayo Clinic, Rochester, MN 55905 USA

M.W. Urban[Member, IEEE],
Department of Physiology and Biomedical Engineering, Mayo Clinic, College of Medicine, Rochester, MN 55905 USA

M. Fatemi[Senior Member, IEEE], and
Department of Physiology and Biomedical Engineering, Mayo Clinic, College of Medicine, Rochester, MN 55905 USA

J.F. Greenleaf[Life Fellow, IEEE]
Department of Physiology and Biomedical Engineering, Mayo Clinic, College of Medicine, Rochester, MN 55905 USA

F.G. Mitri: mitri@lanl.gov; M.W. Urban: urban.matthew@mayo.edu; M. Fatemi: fatemi@mayo.edu; J.F. Greenleaf: jfg@mayo.edu

Abstract

This paper reports shear stiffness and viscosity “virtual biopsy” measurements of three excised non-cancerous human prostates using shearwave dispersion ultrasound vibrometry (SDUV) *in vitro*. Improved methods for prostate guided-biopsy are required to effectively guide needle biopsy to the suspected site. In addition, tissue stiffness measurement helps identifying a suspected site to perform biopsy because stiffness has been shown to correlate with pathology. More importantly, early detection of prostate cancer may guide minimally-invasive therapy and eliminate insidious procedures. In this work, “virtual” biopsies were taken in multiple locations in three excised prostates. Then, SDUV shear elasticity and viscosity measurements have been performed at the selected “suspicious” locations within the prostates. SDUV measurements of prostate elasticity and viscosity are generally in agreement with preliminary values reported previously in the literature. It is however important to emphasize that the obtained viscoelastic parameters values are *local*, and not a mean value for the whole prostate.

I. Introduction

Prostate cancer is recognized as one of the most prevalent malignant diseases and is the most commonly diagnosed cancer among men in the U.S. In 2008, an estimated 186 320 men will be diagnosed with prostate cancer and 28 660 men will die of this disease [1]. Quantitative screening for prostate cancer at the early stage will reduce the mortality number, and allows efficient therapies such as brachytherapy or cryosurgery to be undertaken. The gold standard

Correspondence to: F.G. Mitri, mitri@lanl.govmitri@ieee.org.
F.G. Mitri is now with the Acoustics and Sensors Technology Team, Los Alamos National Laboratory Sensors and Electrochemical Devices Group, Los Alamos, NM 87545 USA

is the sextant biopsy technique which is best to diagnose prostate cancer [2, 3]. In most instances, biopsy samples are correlated with the Gleason score [4] in the staging of prostate cancer. However, some data suggested an underestimation in 43.8% of cases and an overestimation in 17% of cases for prostatectomy. Initially, a Digital Rectal Exam (DRE) is used to palpate the prostate before any biopsy is taken. An overview of studies of screening suggests that DRE alone detects less than 60% of prevalent prostate cancers [5], while a meta-analysis of DRE as screening test reveals overall sensitivity, specificity, and positive predictive value at 53.2%, 83.6%, and 17.8%, respectively [6]. Sensitivity and specificity of PSA screening alone is also questionable. Specificity has been estimated at around 90% on the first screening round but declines with increasing age and the presence of benign prostatic hypertrophy (BPH) [7]. Despite evident drawbacks of both methods, the combination of DRE and PSA do appear to improve the screening; in a large study of volunteers, 26% more cancers were detected than PSA alone [8]. On the other hand, some data have shown that the combinations of DRE along with the interpretation of prostate biopsy are not accurate clinical tools for defining the location and extent of prostatic carcinoma [9].

In practice, real-time monitoring of prostate imaging and needle biopsy guiding with conventional transrectal ultrasound (TRUS) as well as Power Doppler transrectal ultrasound imaging had been successful to improve prostate cancer detection rate [10, 11]. However, significant number of cancers were still missed on initial biopsy [12]. It is therefore of some importance to work out novel tissue characterization tools and technologies to help guiding needle biopsy in the prostate.

The difference in the elasticity of tumors and normal (healthy) tissues [13–17] has provided the impetus to develop elasticity imaging techniques [18–32] based on the quantitative measurement of their viscoelastic parameters. However, at present, there is no gold standard for stiffness and viscosity measurements in soft biological tissues. Although Magnetic Resonance Elastography (MRE) has shown significant capabilities in prostate cancer detection [18, 33], this technology is expensive, thus less likely to see wide clinical applications and may not be widely available for general screening. On the other hand, ultrasound-based elastography methods for the prostate include a variety of approaches [19–26, 34, 35], and due to both efficiency in delineating prostate boundaries and low cost, developments of new ultrasonic techniques are still very active. Although these tools are valuable in detecting abnormal prostate lesions in clinical practice, they are however inadequate when abnormalities are not confined to a local region and there is no normal background tissue to provide contrast. In addition, estimation of elastic parameters largely depends on the boundary conditions. Such circumstances require quantitative methods, where tissue elasticity is inversely solved in unit of Pascal. Considerable efforts have been therefore directed to developing quantitative methods in recent years. Several groups have proposed the use of shear wave propagation speed for quantifying tissue stiffness [36–41]. However, tissue viscosity is neglected in these methods, and this omission can cause bias in the estimation of tissue elasticity because recent studies suggest that viscosity is another useful index of tissue health [42, 43]. Supersonic shear imaging has some potential to solve quantitatively both tissue elasticity and viscosity [44]. However, this technique requires super fast imaging, which is not compatible with current commercial ultrasound scanners. Therefore, a quantitative method that mimics DRE, but with enhanced sensitivity, specificity and reduction of the sampling error, might consequently lead to a better biopsy sampling and staging prostate diseases.

A newly emerging technology called Shearwave Dispersion Ultrasound Vibrometry (SDUV) [45], that quantifies both elasticity and viscosity by evaluating dispersion of shear wave propagation speed, has been successfully used to characterize *in vitro* bovine and

porcine striated muscle and *in vivo* swine liver tissue [45], and may potentially improve evaluation of prostate mechanical parameters and guide needle biopsy to the appropriate suspected site. The purpose of this study is therefore directed toward evaluating the feasibility of using conventional ultrasound imaging to locate a suitable site for SDUV measurements of elasticity and viscosity in the prostate.

II. METHODS

A. Principle of SDUV

In SDUV [45], an external localized ultrasound force is applied to generate harmonic shear waves that propagate outward from the vibration center. For a complete description of the method, the reader is referred to [45, 46].

For a homogenous material described by the Voigt model the shear wave speed c_s depends on its angular frequency ω_s [47, 48] such that

$$c_s(\omega_s)=\sqrt{2\left(\mu_1^2+\omega_s^2\mu_2^2\right)/\rho\left(\mu_1+\sqrt{\mu_1^2+\omega_s^2\mu_2^2}\right)}, \tag{1}$$

where ρ, μ_1 and μ_2 are the density, shear elasticity and shear viscosity of the medium, respectively. The external localized force is generated by a “Push” beam (Fig. 1) that transmits repeated tone bursts of ultrasound. Typically, a push sequence consists of 10 tone bursts that exert a force of constant amplitude every 10 ms.

A shear wave propagating outwards from the vibration center can be monitored by a “Detect” beam operating in pulse-echo mode at two locations along the propagation path. The propagation speed of a shear wave is estimated by tracking its phase change over the distance it has propagated. The phase velocity of the shear wave is characterized at a number of selected frequencies to assess the dispersion of its wave velocity.

The shear wave speed is calculated using the formula [45]:

$$c_s(\omega_s)=\omega_s\Delta r/\Delta\varphi_s, \tag{2}$$

where $\Delta\varphi_s = \varphi_1 - \varphi_2$ is the phase change over the traveled distance Δr, φ_1 and φ_2 are the phases at the “Detect” points “1” and “2”, respectively. The variation of c_s versus frequency is then fit by (1) to inversely solve for elasticity and viscosity.

B. Experiments

Three freshly excised human prostates from cadavers were placed in a saline water solution for 0.5 hour while transported and then embedded in separate gel phantoms. The water-based gelatin was made using 300 Bloom gelatin and glycerol (Sigma-Aldrich, St. Louis, MO) using a concentration of 10% by volume for both components. Potassium sorbate (Sigma-Aldrich, St. Louis, MO) was added as a preservative at 10 g/L. Each gel block was placed in a water tank and scanned by conventional B-mode ultrasound at 4 MHz with a Vivid 7 GE commercial ultrasound machine. For each prostate, five regions were selected within the B-scan image (colored circles in Fig. 2-(b)) in which propagation of shear waves was detected at 3 different positions (shown as white dots within each region) corresponding to 3 measurements, ≈1 mm apart, at 50 Hz and its higher harmonics (100 to 400 Hz). The phase of shear waves at frequencies 50–400 Hz was estimated from these vibration-time

records after computing a Fast Fourier Transform (FFT) on the time-domain displacement signal.

For the SDUV measurements on the excised prostates, two separate transducers were used in the experiments. The pulse sequence was decomposed into two groups: the push pulses and the detect pulses. The push pulses drove a “Push” transducer to generate the push beams at a fixed point within the prostatic region, while the detect pulses drove a separate “Detect” transducer (positioned beside the push transducer) to generate the detect beams. The “Detect” transducer is mechanically translated perpendicularly to the beam axis to track the shear wave at multiple points within each region. Although two separate transducers were used in the experimental setup, the envisioned (prospective) operation of SDUV for measuring elasticity and viscosity of the prostate in a *clinical setting* is as follows: initially an image the prostate will be taken using B-mode TRUS to locate a site for SDUV measurements. Then, a location of interest will be selected within the B-mode ultrasound image and the ultrasound “Push” transducer temporarily switches to SDUV mode (using the *same* probe) to measure prostate elasticity and viscosity at the specified location (Fig. 1). All the procedures used on the excised prostates were approved by the Mayo Clinic Institutional Review Board (protocol ID 06-003629).

After locating suitable regions (far from the intraprostatic calcifications shown on the X-ray image (Fig. 2-(a))) simulating suspected sites for needle biopsy, and denoted by circles in the B-mode ultrasound image, SDUV measurements were then performed. A diagram of the experimental setup is shown in Figure 3. The transducer used for generating the shear wave was a 3 MHz spherically focused transducer with a focal length of 10 cm and diameter of 45 mm that was assembled in-house. The transducer used for detection was a 5 MHz spherically focused transducer with focal length of 5 cm and diameter of 12.5 mm (i3-0508-R-SU, Olympus NDT, Waltham, MA). The push transducer was driven with a 3 MHz tone-burst of length 0.3 ms (HP33120A, Agilent, Santa Clara, CA) and the signal was amplified by a custom-made power amplifier with a gain of 40 dB. This tone-burst was repeated at a pulse repetition frequency (PRF_p) equal to 50 Hz where the subscript “p” refers to the push. The detect transducer was driven with a pulser/receiver (5072PR, Olympus NDT, Waltham, MA). The output signal was filtered and amplified using a logarithmic amplifier. The pulse-echo operation was repeated at a pulse repetition frequency (PRF_d where the subscript “d” refers to the detection) equal to 1.6 kHz for prostates 1 and 2 and 2.0 kHz for prostate 3, and echoes were recorded at 100 MHz sampling rate. The duration for a single measurement was 200 ms.

The push and detection transducers were co-focused before the experiment using a small steel sphere on a membrane. After this co-focus was established, the phantom was moved in between the transducers and measurements were made. The push transducer remained in a fixed position and the detection transducer was moved in 0.5 mm increments for 5 mm to vary the value of Δr used in (2).

Motion detection was performed using cross-spectral analysis [49] and the phase at 50–400 Hz was evaluated in 50 Hz increments using the aforementioned FFT-based method. The phase versus distance was assessed and data with linear phase was used to calculate the shear wave speed. The dispersive shear wave speed was then fit to (1) to estimate the viscoelastic material properties.

III. RESULTS AND DISCUSSION

Figure 2 shows an X-ray fluoroscopic image (a) and conventional B-mode ultrasound image (b) of one of the prostates embedded in a gel phantom. In (a), clusters of calcifications

appear as bright spots. The urethra is also shown as a black dot at the center of the image. In the B-mode ultrasound image at 4 MHz (i.e. (b)), 5 regions far from the calcifications and denoted by colored circles were selected for appropriate SDUV measurements. Detection points are shown as white dots in (b).

Figure 4-(a) shows the displacement induced by the "Push" beam as measured by the "Detect" beam for one measurement. The "Push" beam stimulated the propagation of shear waves that were detected at three different locations (white dots in Fig. 2-(b)), 1 mm apart, within the prostate. The phase of shear waves at frequencies 50–400 Hz was estimated from these vibration-time records by the Kalman filter and shown in Figure 4-(b), which demonstrates that the shear wave phase changes *linearly* (as assumed with Eq.(2)) with propagation distance for all frequencies studied. The shear wave speed, shown as circles in Fig. 4-(c), is calculated using the phase information in Fig. 4-(b). The solid line is the fit by Eq.(1) to the measured shear wave speeds which gives μ_1 = 1.80 kPa and μ_2 = 1.09 Pa·s. The means and standard deviations of prostate shear wave speeds obtained from 5 consecutive SDUV measurements are shown in Fig. 4-(d) that shows good repeatability of wave speeds and close values to those in Fig. 4-(c).

Additional multiple SDUV "virtual biopsies" measurements have been performed within each prostate over 5 different regions. In each region, separate measurements were performed at 3 different positions (ranging from 1 to 5 mm deep through the tissue). As expected, the results showed different values for stiffness and viscosity. The measurements were made 4–5 times to evaluate the precision of the measurements, and the mean and standard deviations of the measurements are summarized in Table 1.

The mean values of μ_1 and μ_2 for the three prostates ranged from 1.31–12.81 kPa and 1.10–6.82 Pa·s, respectively. The range of these values may have their origins in heterogeneity of the tissue. For most measurements, the precision was very good.

There exist previous literature reports on measuring the prostate elasticity using MRE for 7 healthy human volunteers *in vivo* [50] and in a canine model. The *mean* shear elasticity values obtained with MRE on human prostates [50] in the central and peripheral prostatic portion were $\mu_1 = 2.2 \pm 0.3$ kPa and $\mu_1 = 3.3 \pm 0.5$ kPa, respectively. In MRE, measurement of the elastic modulus was done at a *fixed* excitation (low) frequency, i.e. 65 Hz. At this (low) frequency, the effects of viscosity may generally be ignored as shown by Eq.(1). Thus the shear wave speed in this limit is given from Eq.(1) as

$$c_s(\omega_s \to 0) \approx \sqrt{\mu_1/\rho}. \tag{3}$$

Assuming that the density for tissue approximates water ($\rho \approx 1000\ kg/m^3$), the value of the *mean* shear wave speed ranges from ≈1.48 *m/s* to 1.82 *m/s*, values that are in the range of the SDUV measurements. On the other hand, the study on the canine model [33] reports mean shear stiffness values ranging from $\mu_1 = 5.3 \pm 1.4$ to $\mu_1 = 6.3 \pm 1.7$. The overall SDUV results showed higher shear stiffness values from the *in vivo* MRE results [50] but closer values to the *in vivo* study on the canine model [33]. The higher values for the stiffness may be attributed to the fact that the prostate glands were excised and had no blood perfusion. In addition, the choice of the fitting model is of particular importance since it determines the estimation process of shear stiffness and viscosity. However, at the present time, it is not yet established which model is the most appropriate to describe the response of soft tissues, especially the prostate. In these results, the excellent fits between (1) and the shear wave

speed dispersion measured in the prostates suggest that the Voigt dispersion model is sufficient, at least for the frequency range used here.

In the experiments two separate transducers were used (Fig. 3). However, the use of a single linear transrectal array transducer (as shown in Fig. 1) will be more useful and especially relevant for a clinical setting. At the present time, we have no access to control the operation of a commercial array transducer, but this will be the subject of future investigations.

An advantage of this method is that SDUV virtual biopsies are fast (less than 0.1 s) and multiple virtual biopsies could be done to aid in actual biopsy placement. Moreover, the proposed method is economical (this is a modification of current ultrasound scanners and therefore will be relatively easy to implement) and compatible with existing commercial ultrasound scanners. Hence, it may potentially operate in clinical ultrasound examinations. For the discussion of other advantages and limitations of SDUV, the reader is kindly referred to [45].

IV. Conclusion

This study showed the feasibility of using B-mode ultrasound imaging to locate a specific region within excised human prostates *in vitro* and perform SDUV “virtual biopsy” measurements of prostate elasticity and viscosity. Results from this preliminary study are generally in agreement with initial values reported previously in the literature. It is important to emphasize that SDUV measurements are local, and not an average value of elasticity for the whole prostate as in MRE. Future work will be directed toward *in vivo* measurements in a clinical setting using TRUS and suitable modification of the system to perform “virtual biopsy” measurements in a clinical setting.

References

1. Jemal A, Siegel R, Ward E, Hao Y, Xu J, Murray T, Thun MJ. Cancer Statistics, 2008. CA Cancer J Clin. 2008; 58(2):71–96. [PubMed: 18287387]
2. Hodge KK, McNeal JE, Terris MK, Stamey TA. Random systematic versus directed ultrasound guided transerctal core biopsies of the prostate. Journal of Urology. 1989; 141:71–75. [PubMed: 2659827]
3. Hodge KK, McNeal JE, Stamey TA. Ultrasound guided transrectal core biopsies of the palpably abnormal prostate. Journal of Urology. 1989; 142:66–70. [PubMed: 2659826]
4. Gleason D, Mellinger GT. a. T. V. A. c. U. R. Group. Prediction of prognosis for prostatic adenocarcinoma by combined histologic grading and clinical staging. Journal of Urology. 1974; 111:58–64. [PubMed: 4813554]
5. U.S. Preventive Services Task Force. Screening for Prostate Cancer: Recommendation and Rationale. Ann Intern Med. 2002; 137(11):915–916. [PubMed: 12458992]
6. Mistry K, Cable G. Meta-Analysis of Prostate-Specific Antigen and Digital Rectal Examination as Screening Tests for Prostate Carcinoma 10.3122/jabfm.16.2.95. J Am Board Fam Pract. 2003; 16(2):95–101. [PubMed: 12665174]
7. Mettlin C, Murphy GP, Babaian RJ, Chesley A, Kane RA, Littrup PJ, Mostofi FK, Ray PS, Shanberg AM, Toi A. The results of a five-year early prostate cancer detection intervention. Cancer. 1996; 77(1):150–159. [PubMed: 8630923]
8. Catalona WJ, Richie JP, Ahmann FR, Hudson MA, Scardino PT, Flanigan RC, Dekernion JB, Ratliff TL, Kavoussi LR, Dalkin BL, Waters WB, Macfarlane MT, Southwick PC. Comparison of Digital Rectal Examination and Serum Prostate-Specific Antigen in the Early Detection of Prostate-Cancer - Results of a Multicenter Clinical-Trial of 6,630 Men. Journal of Urology. 1994; 151(5): 1283–1290. [PubMed: 7512659]

9. Obek C, Louis P, Civantos F, Soloway MS. Comparison of digital rectal examination and biopsy results with the radical prostatectomy specimen. Journal of Urology. 1999; 161(2):494–498. [PubMed: 9915434]
10. Donnelly EF, Geng L, Wojcicki WE, Fleischer AC, Hallahan DE. Quantified power Doppler US of tumor blood flow correlates with microscopic quantification of tumor blood vessels. Radiology. 2001; 219(1):166–170. [PubMed: 11274552]
11. Remzi M, Dobrovits M, Reissigl A, Ravery V, Waldert M, Wiunig C, Fong YK, Djavan B. Can power Doppler enhanced transrectal ultrasound guided biopsy improve prostate cancer detection on first and repeat prostate biopsy? European Urology. 2004; 46(4):451–456. [PubMed: 15363559]
12. Norberg M, Egevad L, Holmberg L, Sparen P, Norlen BJ, Busch C. The sextant protocol for ultrasound-guided core biopsies of the prostate underestimates the presence of cancer. Urology. 1997; 50(4):562–566. [PubMed: 9338732]
13. Krouskop TA, Wheeler TM, Kallel F, Garra BS, Hall T. Elastic moduli of breast and prostate tissues under compression. Ultrasonic Imaging. 1998; 20(4):260–274. [PubMed: 10197347]
14. Phipps S, Yang THJ, Habib FK, Reuben RL, McNeill SA. Measurement of tissue mechanical characteristics to distinguish between benign and malignant prostatic disease. Urology. 2005; 66(2):447–450. [PubMed: 16098374]
15. Jalkanen V, Andersson BM, Bergh A, Ljungberg B, Lindahl OA. Resonance sensor measurements of stiffness variations in prostate tissue in vitro - a weighted tissue proportion model. Physiological Measurement. 2006; 27(12):1373–1386. [PubMed: 17135706]
16. Jalkanen V, Andersson BM, Bergh A, Ljungberg B, Lindahl OA. Prostate tissue stiffness as measured with a resonance sensor system: a study on silicone and human prostate tissue in vitro. Medical & Biological Engineering & Computing. 2006; 44(7):593–603. [PubMed: 16937195]
17. Hoyt K, Castaneda B, Zhang M, Nigwekar P, di Sant'Agnese PA, Joseph JV, Strang J, Rubens DJ, Parker KJ. Tissue elasticity properties as biomarkers for prostate cancer. Cancer Biomarkers. 2008; 4(4–5):213–225. [PubMed: 18957712]
18. Lorenzen J, Sinkus R, Adam G. Elastography: Quantitative imaging modality of the elastic tissue properties. Rofo-Fortschritte Auf Dem Gebiet Der Rontgenstrahlen Und Der Bildgebenden Verfahren. 2003; 175(5):623–630.
19. Rubens DJ, Hadley MA, Alam SK, Gao L, Mayer RD, Parker KJ. Sonoelasticity Imaging of Prostate-Cancer - in-Vitro Results. Radiology. 1995; 195(2):379–383. [PubMed: 7724755]
20. Cochlin DL, Ganatra RH, Griffiths DFR. Elastography in the detection of prostatic cancer. Clinical Radiology. 2002; 57(11):1014–1020. [PubMed: 12409113]
21. Souchon R, Rouviere O, Gelet A, Detti V, Srinivasan S, Ophir J, Chapelon JY. Visualisation of hifu lesions using elastography of the human prostate in vivo: Preliminary results. Ultrasound in Medicine and Biology. 2003; 29(7):1007–1015. [PubMed: 12878247]
22. Curiel L, Souchon R, Rouviere O, Gelet A, Chapelon JY. Elastography for the follow-up of high-intensity focused ultrasound prostate cancer treatment: Initial comparison with MRI. Ultrasound in Medicine and Biology. 2005; 31(11):1461–1468. [PubMed: 16286025]
23. Konig K, Scheipers U, Pesavento A, Lorenz A, Ermert H, Senge T. Initial experiences with real-time elastography guided biopsies of the prostate. Journal of Urology. 2005; 174(1):115–117. [PubMed: 15947593]
24. Egorov V, Ayrapetyan S, Sarvazyan AP. Prostate mechanical imaging: 3-D image composition and feature calculations. Ieee Transactions on Medical Imaging. 2006; 25(10):1329–1340. [PubMed: 17024836]
25. Weiss RE, Egorov V, Ayrapetyan S, Sarvazyan N, Sarvazyan A. Prostate mechanical imaging: A new method for prostate assessment. Urology. 2008; 71(3):425–429. [PubMed: 18342178]
26. Zhang M, Nigwekar P, Castaneda B, Hoyt K, Joseph JV, Agnese AD, Messing EM, Strang JG, Rubens DJ, Parker KJ. Quantitative characterization of viscoelastic properties of human prostate correlated with histology. Ultrasound in Medicine and Biology. 2008; 34(7):1033–1042. [PubMed: 18258350]
27. Greenleaf JF, Fatemi M, Insana MF. Selected methods for imaging elastic properties of biological tissues. Annual Review of Biomedical Engineering. 2003; 5:57–78.

28. Pellot-Barakat C, Sridhar M, Lindfors KK, Insana MF. Ultrasonic elasticity imaging as a tool for breast cancer diagnosis and research. Current Medical Imaging Reviews. 2006; 2(1):157–164.
29. Mitri FG, Davis BJ, Greenleaf JF, Fatemi M. In vitro comparative study of vibro-acoustography versus pulse-echo ultrasound in imaging permanent prostate brachytherapy seeds. Ultrasonics. 2009; 49(1):31–38. [PubMed: 18538365]
30. Mitri FG, Trompette P, Chapelon JY. Improving the use of vibro-acoustography for brachytherapy metal seed imaging: A feasibility study. IEEE Transactions on Medical Imaging. 2004; 23(1):1–6. [PubMed: 14719682]
31. Mitri FG, Davis BJ, Urban MW, Alizad A, Greenleaf JF, Lischer GH, Wilson TM, Fatemi M. Vibro-acoustography Imaging of Permanent Prostate Brachytherapy seeds in an excised human prostate - Preliminary Results and Technical Feasibility. Ultrasonics. 2009; 49(3):389–394. [PubMed: 19062061]
32. Mitri FG, Davis BJ, Alizad A, Greenleaf JF, Wilson TM, Mynderse LA, Fatemi M. Prostate Cryotherapy Monitoring Using Vibroacoustography: Preliminary Results of an Ex Vivo Study and Technical Feasibility. IEEE Transactions on Biomedical Engineering. 2008; 55(11):2584–2592. [PubMed: 18990628]
33. Chopra R, Arani A, Huang YX, Musquera M, Wachsmuth J, Bronskill M, Plewes D. In Vivo MR Elastography of the Prostate Gland Using a Transurethral Actuator. Magnetic Resonance in Medicine. 2009; 62(3):665–671. [PubMed: 19572390]
34. Pallwein L, Mitterberger M, Struve P, Pinggera G, Horninger W, Bartsch G, Aigner F, Lorenz A, Pedross F, Frauscher F. Real-time elastography for detecting prostate cancer: preliminary experience. Bju International. 2007; 100(1):42–46. [PubMed: 17552952]
35. Ginat DT, Destounis SV, Barr RG, Castaneda B, Strang JG, Rubens DJ. US Elastography of Breast and Prostate Lesions. Radiographics. 2009; 29(7):2007–2016. [PubMed: 19926759]
36. Sarvazyan AP, Rudenko OV, Swanson SD, Fowlkes JB, Emelianov SY. Shear wave elasticity imaging: A new ultrasonic technology of medical diagnostics. Ultrasound in Medicine and Biology. 1998; 24(9):1419–1435. [PubMed: 10385964]
37. Sandrin L, Tanter M, Catheline S, Fink M. Shear modulus imaging with 2-D transient elastography. IEEE Transactions on Ultrasonics Ferroelectrics and Frequency Control. 2002; 49(4):426–435.
38. Nightingale K, McAleavey S, Trahey G. Shear-wave generation using acoustic radiation force: In vivo and ex vivo results. Ultrasound in Medicine and Biology. 2003; 29(12):1715–1723. [PubMed: 14698339]
39. Wu Z, Taylor LS, Rubens DJ, Parker KJ. Sonoelastographic imaging of interference patterns for estimation of the shear velocity of homogeneous biomaterials. Physics in Medicine and Biology. 2004; 49(6):911–922. [PubMed: 15104315]
40. Konofagou EE. Quo vadis elasticity imaging? Ultrasonics. 2004; 42(1–9):331–336. [PubMed: 15047307]
41. Maleke C, Konofagou EE. Harmonic motion imaging for focused ultrasound (HMIFU): a fully integrated technique for sonication and monitoring of thermal ablation in tissues. Physics in Medicine and Biology. 2008; 53(6):1773–1793. [PubMed: 18367802]
42. Huwart L, Peeters F, Sinkus R, Annet L, Salameh N, ter Beek LC, Horsmans Y, Van Beers BE. Liver fibrosis: non-invasive assessment with MR elastography. Nmr in Biomedicine. 2006; 19(2): 173–179. [PubMed: 16521091]
43. Salameh N, Peeters F, Sinkus R, Abarca-Quinones J, Annet L, ter Beek LC, Leclercq I, Van Beers BE. Hepatic viscoelastic parameters measured with MR elastography: Correlations with quantitative analysis of liver fibrosis in the rat. Journal of Magnetic Resonance Imaging. 2007; 26(4):956–962. [PubMed: 17896384]
44. Bercoff J, Tanter M, Fink M. Supersonic shear imaging: A new technique for soft tissue elasticity mapping. IEEE Transactions on Ultrasonics Ferroelectrics and Frequency Control. 2004; 51(4): 396–409.
45. Chen SG, Urban MW, Pislaru C, Kinnick R, Zheng Y, Yao AP, Greenleaf JF. Shearwave Dispersion Ultrasound Vibrometry (SDUV) for Measuring Tissue Elasticity and Viscosity. IEEE Transactions on Ultrasonics Ferroelectrics and Frequency Control. 2009; 56(1):55–62.

46. Chen SG, Fatemi M, Greenleaf JF. Quantifying elasticity and viscosity from measurement of shear wave speed dispersion. Journal of the Acoustical Society of America. 2004; 115(6):2781–2785. [PubMed: 15237800]

47. Ostreicher HL. Field and Impedance of an Oscillating Sphere in a Viscoelastic Medium with an Application to Biophysics. Journal of the Acoustical Society of America. 1951; 23(6):707–714.

48. Yamakoshi Y, Sato J, Sato T. Ultrasonic imaging of internal vibration of soft tissue under forced vibration. Ultrasonics, Ferroelectrics and Frequency Control, IEEE Transactions on. 1990; 37(2): 45–53.

49. Hasegawa H, Kanai H. Improving accuracy in estimation of artery-wall displacement by referring to center frequency of RF echo. IEEE Transactions on Ultrasonics Ferroelectrics and Frequency Control. 2006; 53(1):52–63.

50. Kemper J, Sinkus R, Lorenzen J, Nolte-Ernsting C, Stork A, Adam G. MR elastography of the prostate: Initial in-vivo application. Rofo-Fortschritte Auf Dem Gebiet Der Rontgenstrahlen Und Der Bildgebenden Verfahren. 2004; 176(8):1094–1099.

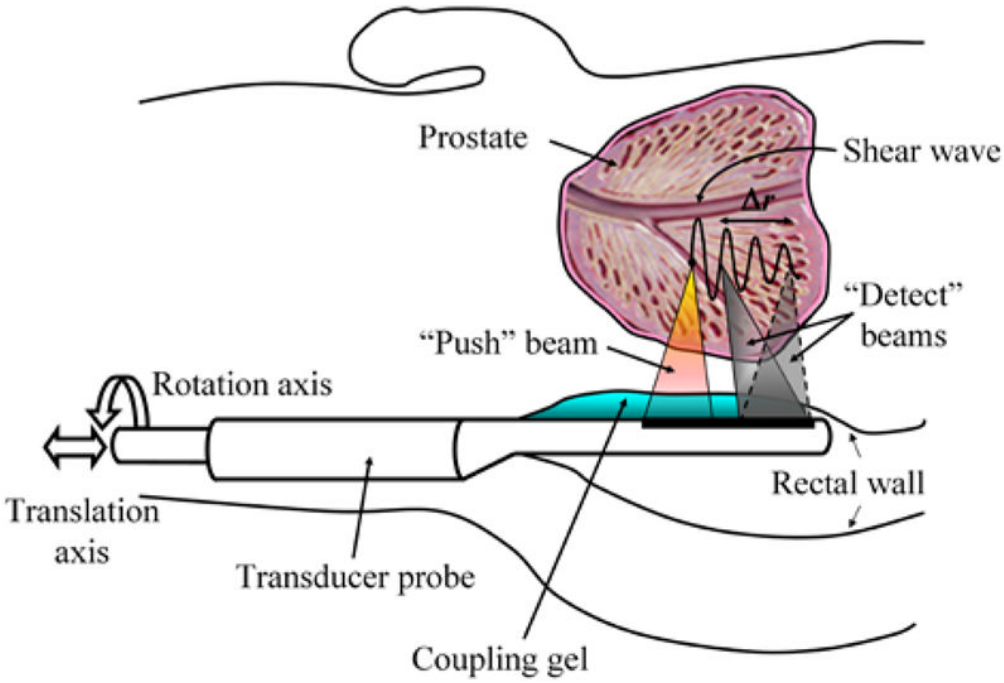

Fig. 1.

A graphic describing the principle of transrectal-SDUV for the measurement of prostate viscoelastic parameters. A harmonic shear wave is produced by a "Push" ultrasound beam, and its propagation is monitored by a separate "Detect" ultrasound beam at two positions using the same probe. The shear wave speed is calculated from its phase φ_1 and φ_2 measured at 2 locations (separated by a distance Δr) along its traveling path.

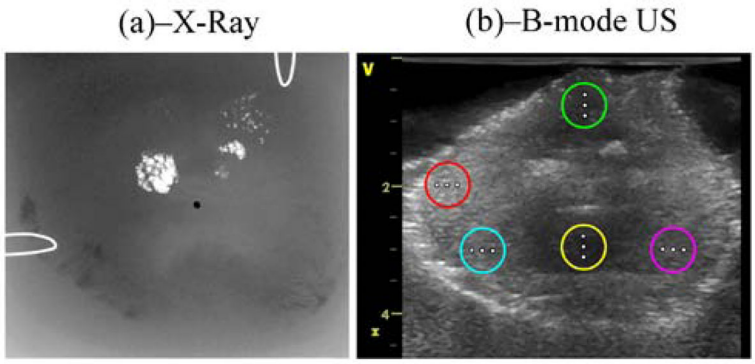

Fig. 2.

Prostate imaging with two modalities: (a) corresponds to an X-ray fluoroscopic image in which clusters of calcifications appear as bright spots. The urethra is also shown as a black dot at the center of the image. (b) corresponds to a conventional B-mode ultrasound image in which 5 regions were selected and shown as colored circles. SDUV excitation points are shown as white dots on the figure. The image size is (HxW≈) 4.5×5 cm^2.

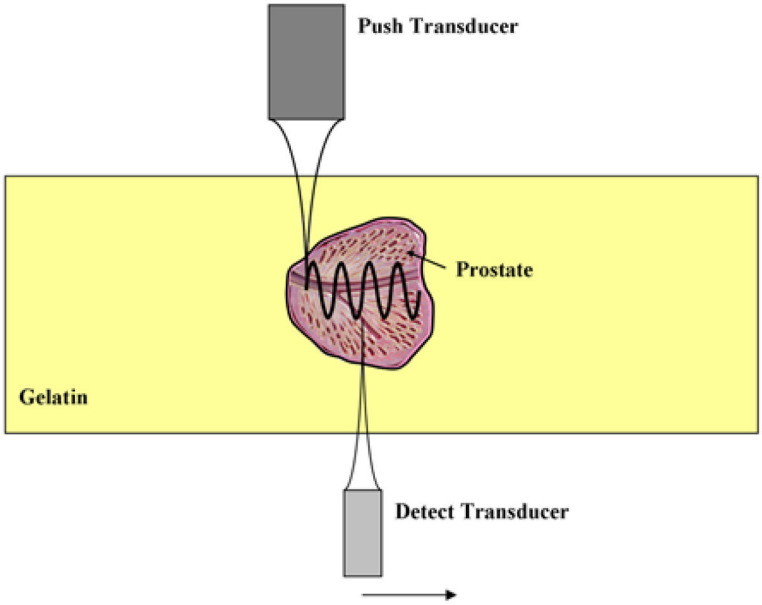

Fig. 3.
Experimental setup for SDUV measurements. The excised prostate was embedded in a gelatin phantom. The push and detect transducers were co-focused before the experiment. The push transducer creates a propagating shear wave and the detect transducer measures the motion at several locations.

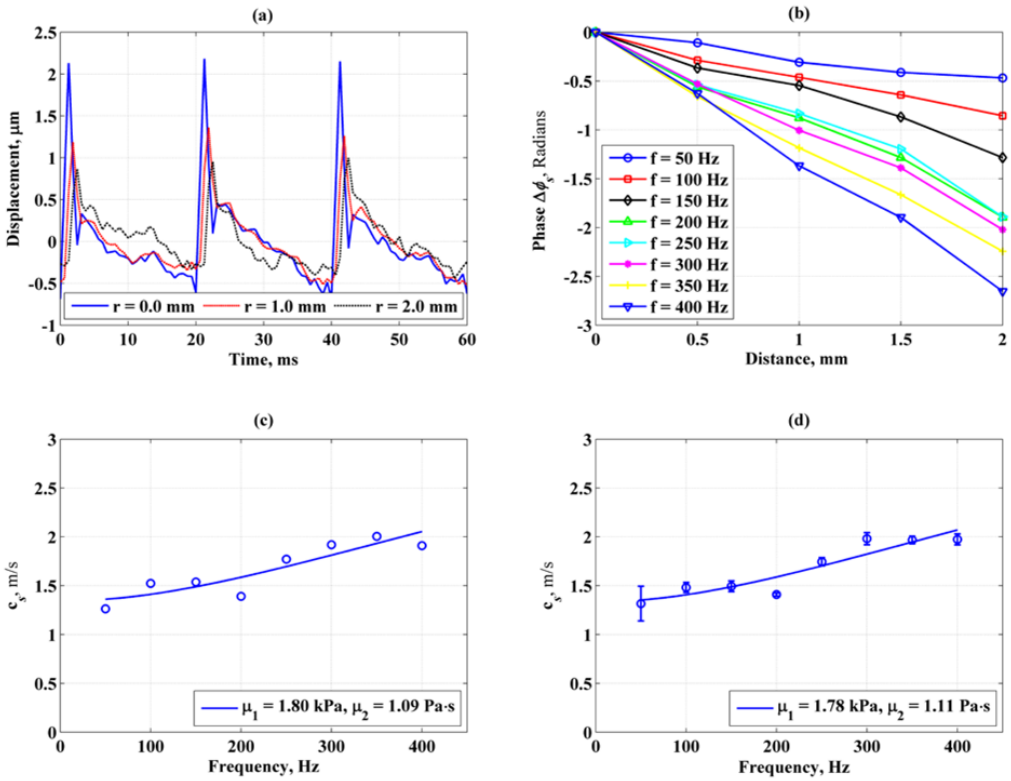

Fig. 4.

Example of an SDUV stiffness and viscosity measurement of an excised human prostate within one single region. (a) & (b): amplitude of displacement and phase of vibration records detected at 3 different locations, 1 mm apart. (c): shear wave speed vs. frequency. The stiffness and viscosity were μ_1 = 1.80 kPa and μ_2 = 1.09 Pa.s, respectively (d): Shear wave speeds calculated from 5 acquisitions to check the repeatability of (c). The mean stiffness and viscosity were μ_1 = 1.78 kPa and μ_2 = 1.11 Pa.s, respectively.

Table 1

Shear stiffness and viscosity measurements from 5 regions within each of the prostates at 3 different positions. One particularly notices the variable differences from one sampling point to another. The values reported are the mean and standard deviation of 5 measurements for each position.

Prostate 1						
Region	μ_1, kPa			μ_2, Pa·s		
	Position 1	Position 2	Position 3	Position 1	Position 2	Position 3
1	12.81 ± 0.88	4.89 ± 0.60	7.07 ± 0.40	4.90 ± 0.56	2.43 ± 0.46	1.85 ± 0.19
2	3.70 ± 0.87	6.52 ± 1.07	2.33 ± 0.42	1.49 ± 0.21	3.48 ± 0.21	2.56 ± 0.11
3	1.73 ± 0.35	1.77 ± 0.18	3.29 ± 0.13	1.47 ± 0.06	1.10 ± 0.05	2.13 ± 0.06
4	3.29 ± 0.50	7.81 ± 0.44	3.07± 0.48	1.14 ± 0.30	4.15 ± 0.19	2.93± 0.18
5	7.23 ± 1.70	4.80 ± 0.33	5.49 ± 1.22	2.91 ± 0.71	2.77 ± 0.15	3.10 ± 0.39

Prostate 2						
Region	μ_1, kPa			μ_2, Pa·s		
	Position 1	Position 2	Position 3	Position 1	Position 2	Position 3
1	7.55 ± 1.39	4.12 ± 1.22	8.27 ± 1.51	2.03 ± 1.57	1.84 ± 1.39	1.09 ± 1.50
2	3.95 ± 0.42	5.40 ± 1.12	5.81 ± 2.07	2.53 ± 0.68	3.62 ± 0.51	3.83 ± 0.53
3	9.98 ± 2.44	12.03 ± 1.18	9.10 ± 2.87	5.51 ± 0.22	4.62 ± 0.87	1.74 ± 2.14
4	3.40 ± 1.02	5.1 ± 0.72	3.82 ± 0.51	2.76 ± 0.17	2.73 ± 0.66	6.82 ± 1.87
5	5.47 ± 1.26	4.25 ± 0.98	4.58 ± 0.85	3.46 ± 1.00	2.58 ± 0.30	2.53 ± 0.32

Prostate 3						
Region	μ_1, kPa			μ_2, Pa·s		
	Position 1	Position 2	Position 3	Position 1	Position 2	Position 3
1	7.04 ± 1.24	4.69 ± 0.40	3.11 ± 1.07	1.98 ± 1.23	2.22 ± 0.42	1.81 ± 0.37
2	7.14 ± 2.30	5.13 ± 0.69	4.02 ± 0.39	5.22 ± 1.03	2.18 ± 0.21	1.62 ± 0.17
3	3.94 ± 0.80	4.81 ± 0.14	3.83 ± 0.38	2.50 ± 0.52	2.26 ± 0.07	1.59 ± 0.53
4	1.31 ± 0.10	2.52 ± 0.12	1.80 ± 0.18	0.19 ± 0.22	0.15 ± 0.57	0.73 ± 0.44
5	7.06 ± 2.65	4.90 ± 0.54	3.90 ± 0.33	5.11 ± 1.16	2.23 ± 0.21	1.68 ± 0.11